AIAA 81-2037R

Flight Test of the 747-JT9D for Airframe Noise

Oscar Kipersztok* and Gautam Sengupta†
Boeing Commercial Airplane Company, Seattle, Washington

This paper describes the method used to isolate the individual airframe noise components and determine their relative contribution to the total noise radiated by a 747 aircraft with JT9D-7A engines at approach. The individual components are isolated using ensemble averaged flight test data. The spectral data are normalized on the basis of altitude, airspeed, temperature, and relative humidity. The noise radiated at approach is reconstructed from addition of individual components and compares very accurately in level, spectral shape, and directivity pattern to the actual flyover. A comparison is made between each individual airframe noise component, their logarithmic sum representing the synthesized total airframe component, and Fink's prediction method. The results of this study show that the landing gear, when isolated from configurations having the flaps retracted, is the major contributor to airframe noise. If the effect of flap deployment was included in the isolation of the landing gear noise component, this result could be altered. No evidence of jet-flap interaction noise is found for the 747-JT9D aircraft.

Introduction

THE study of airframe noise and the identification of its sources is becoming increasingly important, as more of the quieter, high bypass ratio engines are being introduced in the commercial aviation industry. The airframe noise levels representative of civil aircraft at the approach configuration have been shown to be 6-10 EPNdB below the FAR 36 noise rule limits.[1-3]

Airframe noise may be regarded as the contribution of individual noise sources, which can be added to estimate the noise generated by the airframe as a whole, provided there is no significant interaction among the various components. This is the underlying assumption in the commonly acceptable "component approach" to airframe noise prediction.[3] In order to reduce airframe noise, its source components must be identified and quantified.

The present study describes the method used to isolate the individual airframe noise components to determine their relative contribution to the total noise radiated by a 747 aircraft at approach with JT9D-7A engines and partially treated nacelles. The data were obtained during a 747 airframe noise flight test conducted in Glasgow, Mont. in September 1979.

Spectral shapes and directivity patterns are identified for noise radiated from clean airframe, landing gear, leading- and trailing-edge flaps (at three different settings: 30, 25, and 10 deg), and spoilers. For each individual component an attempt is made to characterize the velocity power index which allows the extrapolation of sound pressure levels based on velocity. Fourteen different configurations were tested and are listed in Table 1. The data reduction involves a combination of ensemble averaging the spectra for a number of measurements made during the course of a single flyover, as well as measurements of repeated flyovers for the same configuration. The use of the ensemble average technique results in a considerable increase in the statistical confidence of the data.

Presented as Paper 81-2037 at the AIAA 7th Aeroacoustics Conference, Palo Alto, Calif., Oct. 5-7, 1981; submitted Oct. 16, 1981; revision received April 8, 1982.

*Specialist Engineer. Member AIAA.
†Principal Engineer. Associate Fellow AIAA.

Flight Test Program

The 747 (RA001) Aircraft

The aircraft used in the Glasgow flight test is a Boeing-owned 747-100 (serial No. RA001), powered by JT9D-7A engines with partially treated nacelles and it is shown in Fig. 1. The range of weights at which the different configurations were flown was from 477,000 to 566,000 lb. The high lift devices installed on the wings consist of triple-slotted trailing-edge flaps, leading-edge slats, and six spoilers on the upper surface of the wing (Fig. 2). There are four main landing gear units fitted with four wheels each and the nose landing gear unit carrying two wheels (Fig. 3).

During normal approach conditions, the position of the leading-edge slats is a function of the flap angle setting. In this test, except for the 0-deg flap, all other configurations had the leading-edge slats deployed. The specification of spoilers extended meant that both the inboard and outboard spoilers were extended to their maximum angles (25 and 45 deg, respectively) and when the gear were deployed, both the nose and main landing gear units were down.

Data Acquisition System

A flyover noise analysis program was used to ensemble average the one-third-octave band spectra covering a frequency range from 50 Hz to 10 kHz. The program required three kinds of data inputs: acoustic, airplane performance, and weather data.

Measurements were made with an array of seven microphones spaced 210 ft apart and flush mounted to the surface of the runway in order to eliminate ground reflection irregularities in the spectra. These microphones measure sound pressure levels augmented 6 dB relative to free field. The type of microphones used were B&K 4166, 0.5-in. diam with grid.

Airplane performance data were recorded onboard the aircraft, where engine, airplane, and flight parameters were monitored. The test airplane was also equipped with an Airplane Positioning and Camera System (APACS) for determining overhead time, sideline deviation, and altitude from specified target stations along the runway. A synchronization system was used to correlate the acoustic and airplane performance data.

Weather data were recorded from two sources: a 10-m tower which provided surface temperature and relative humidity, and a light aircraft which flew at repeated intervals during the test, equipped with weather recording in-

Table 1 Fourteen flight configurations with averaged values of the physical parameters of interest.

Configuration	Flap, deg	Gear	True airspeed, knots	Engine power, rpm	Engine attitude, deg	Climb gradient, deg	Weight, $\times 10^3$ lb	Angle of attack, deg	Mach No.
1	30	Down	199.3	2408.3	2.1	−4.7	543.7	4.8	0.303
2	30	Down	196.4	998.1	2.4	−7.6	537.4	7.9	0.298
3	30	Down	145.4	934.8	2.6	−6.1	531.3	6.7	0.221
4	25	Down	189.1	2148.1	0.6	−3.7	531.4	2.2	0.287
5	25	Down	196.1	1001.1	−2.3	−6.2	528.4	1.9	0.297
6	10	Up	199.9	1025.1	4.8	−4.9	530.1	7.7	0.302
7	10	Up	193.8	1025.1	3.6	−4.4	516.5	6.0	0.294
8	0	Up	234.1	2424.0	7.7	1.0	513.3	4.8	0.355
9	0	Up	234.3	2171.6	5.8	−0.9	510.9	4.7	0.355
10	0	Up	233.3	1082.0	3.8	−3.1	513.5	4.9	0.353
11	0	Down	237.2	2429.2	6.2	−2.2	507.8	6.4	0.359
12	0	Down	238.4	2157.9	2.4	−3.4	495.9	3.8	0.361
13	0	Down	277.4	2422.9	0.9	−3.2	490.0	2.1	0.420
14	0	Up	278.1	1165.8	1.1	−3.6	493.0	2.7	0.420

Fig. 1 747-JT9D (RA001) aircraft with high lift devices and landing gear deployed during approach.

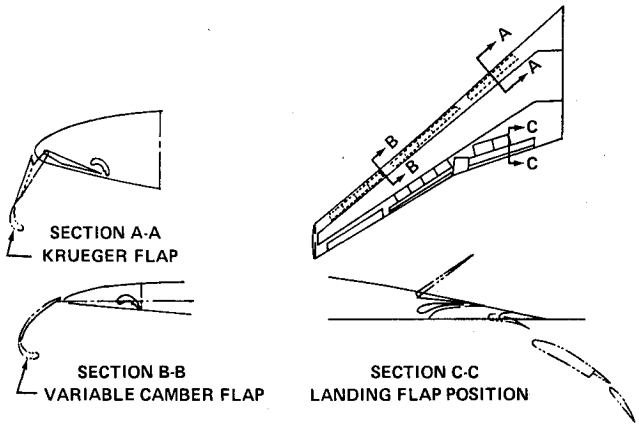

Fig. 2 747 wing with high lift devices.

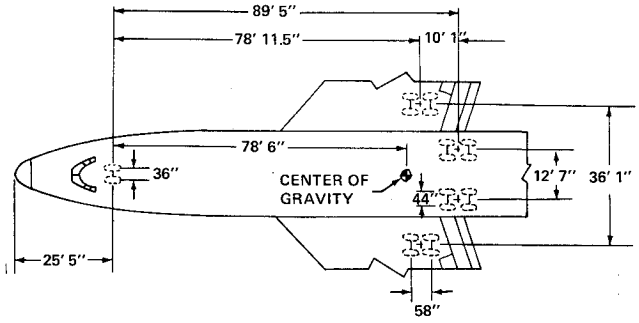

Fig. 3 Landing gear geometry.

strumentation to provide temperatures and relative humidities at various altitudes.

Flight Configurations

Fourteen flight configurations were chosen for the test in order to isolate the different airframe noise components and these are listed in Table 1. The variables defined in the test were the true airspeed, flap angle, landing gear position, and engine rpm. Each configuration was repeated as needed to simulate the target conditions. The values shown in Table 1 are the averages over the repeated flyovers for each configuration.

Data Reduction

The flyover noise analysis program used computes one-third-octave sound pressure level spectra vs noise emission angle. The data were processed using 0.1-s integration time. The SAE atmospheric absorption rates for layered atmosphere were used for atmospheric absorption corrections[6]; and the acoustic levels were extrapolated to reference homogeneous atmosphere (77°F and 70% relative humidity).

Geometric extrapolations were made by applying the inverse square law to normalize the data to a constant altitude of 394 ft (the certification altitude defined at overhead,[7] for the approach configuration), zero sideline offset, zero climb gradient, and an engine attitude of 5.7 deg (the average value from all the flyovers measured). The overall sound pressure levels (OASPL) and perceived noise levels (PNL) were calculated from the one-third-octave spectra.

Data Analysis and Results

Isolation of Airframe Noise Components

A systematic approach was taken in the isolation of airframe noise components. Referring to Table 1, the following components could be identified:

1) "Clean" airframe at 233 and 278 knots from configurations 10 and 14, respectively.

2) Landing gear noise from logarithmic subtraction of configurations 11 and 8 in one case, and of configurations 12 and 9 in another.

3) Leading- and trailing-edge flap noise, at three different settings—30-deg flap noise at 196 and 145 knots from configurations 2 and 3, respectively, 25-deg flap at 196 knots from configuration 5, and 10-deg flap at 194 knots from configuration 6.

4) Spoilers noise by logarithmic subtraction of configuration 6 (with spoilers extended) and configuration 7 (with spoilers retracted).

A repeatability study was performed whereby the spectra of the repeated flyovers were superimposed on a single plot with an accompanying table showing the relevant physical

parameters for the different flyovers with their averages and standard deviations. The study was done to determine whether large variations in these parameters caused any noticeable discrepancies in the spectral levels. Figure 4 shows such repeatability test for configuration 1 at $\theta = 60$-, 90-, and 120-deg directivity angles (as defined with respect to the forward direction of motion). The spectral shape of each configuration was then obtained by averaging the sound pressure levels from the repeated flyovers at each band.

The averaged spectral levels for each configuration were extrapolated to isolate the airframe noise components. Wherever possible, the velocity power index corresponding to each component was found. In a similar manner the directivity patterns (OASPL vs polar angle) were isolated for the various components, and were normalized to a constant polar arc of 394 ft radius with the corresponding corrections for atmospheric absorption.

The clean airframe noise is defined as the noise radiated by an aircraft flying with no flaps or landing gear deployed, and with the engine power setting at idle (1000 rpm). This component is referred to as the "baseline" configuration, since all other components are identified as noise increments relative to clean airframe. The top half of Fig. 5 shows spectra for clean airframe noise at two different airspeeds for $\theta = 60$ deg. Note that clean airframe noise has a broadband component which slowly peaks at 2 kHz and a distinct tone at 315 Hz which appears at 233 knots only. The occurrence of the tone has been observed by other investigators.[1,4,5] The identification of the exact origin and mechanisms causing it to appear are beyond the scope of this paper.

Figure 6 shows the clean airframe noise directivity pattern at the two airspeeds, with peak levels radiated in the forward arc at a polar angle range of 40 to 60 deg. Also shown is a comparison with the clean airframe component predicted by Fink's method for 278 knots.

Since data were available at two different airspeeds (233 and 278 knots), the velocity power index could be determined. The level of the spectra corresponding to 278 knots were extrapolated to 233 knots, separately for several assumed velocity indices, and the two spectra were then compared for different directivity angles. The best collapse between the two spectra was shown to occur at velocity indices from 4 to 5 in the forward arc, where the OASPL peaks. Therefore the mean value of 4.5 was chosen as the velocity index for the clean airframe noise component. The bottom half of Fig. 5 shows the two spectra collapsing after extrapolation using the 4.5 velocity index and compares the spectral shape and level with the clean airframe component predicted by Fink's method. The effect of differences in angle of attack has not been identified because of the lack of adequate data base relating noise radiation to changes in angle of attack.

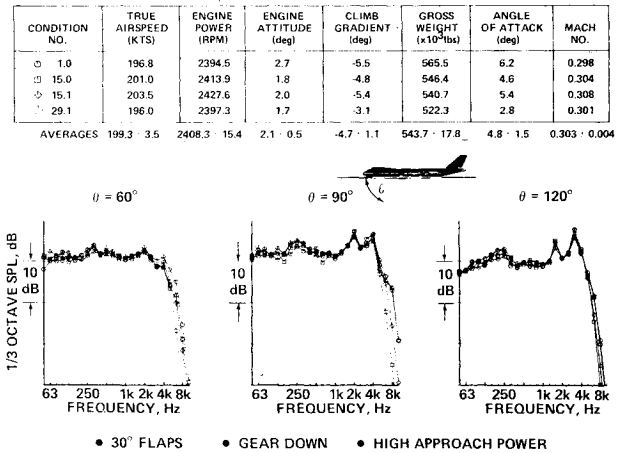

Fig. 4 Repeatability test for configuration 1.

Landing Gear Noise Component

From Table 1, it is seen that the gear noise component can be isolated from two independent subtractions. For clarity, these are denoted cases I and II. In case I, configuration 8 is subtracted from configuration 11, with airspeeds of 234 and 237 knots and engine power settings of 2424 and 2429 rpm, respectively. In case II, configuration 9 is subtracted from configuration 12 with airspeeds similar to case I (234 and 238 knots) and engine power settings lower than those of case I (2172 and 2158 rpm).

Figure 7 shows the isolation of the gear component from case I and its comparison to Fink's prediction at $\theta = 60$ deg.

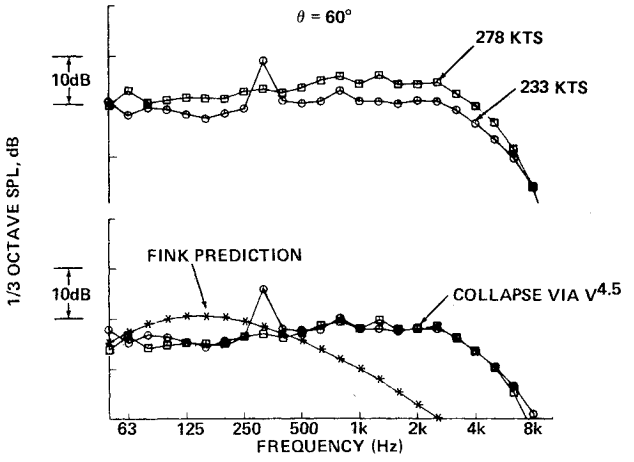

Fig. 5 Clean airframe noise component (0-deg flap, gear up, engine at idle) at two different airspeeds with best collapse shown when spectra extrapolated with a velocity index of 4.5. A comparison shown with Fink's prediction, at $\theta = 60$ deg.

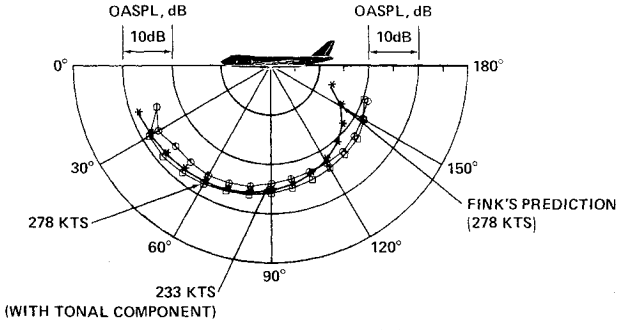

Fig. 6 Directivity pattern of the "clean" airframe component at two airspeeds, and comparison with Fink's prediction for 278 knots.

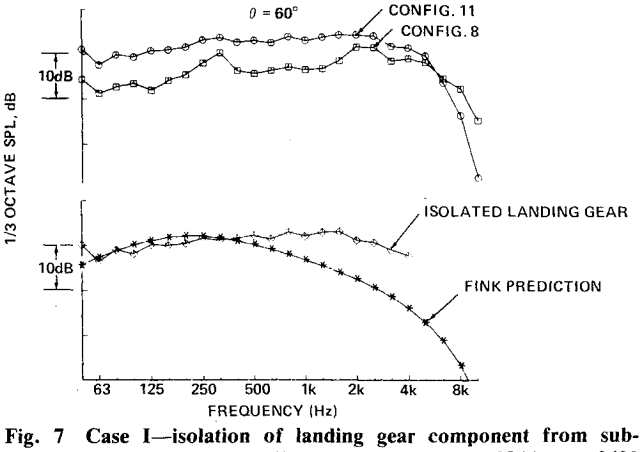

Fig. 7 Case I—isolation of landing gear component from subtraction of configuration 11 (0-deg flap, gear down, 237 knots, 2429 rpm) and configuration 8 (0-deg flap, gear up, 234 knots, 2424 rpm), and comparison with Fink's prediction.

Figure 8 shows the gear component isolated from case II and its superposition with the former case, indicating excellent agreement between the two. This result adds considerable confidence to the validity of the measurements.

Note that in the forward arc, the gear component has a broadband spectrum, slowly peaking at 1.6 kHz. This observation is of significance since sound pressure levels peaking in this range of frequencies have considerable impact on the community noise. However, note that the gear component was isolated from configurations having the trailing-edge flaps retracted. During approach, the flaps are extended to the 30- or 25-deg configurations. The extension of the flaps causes local changes in the flow around the wing gear strut and wheels, which may alter the noise radiated from the landing gear at approach. The extent and nature of this interaction between landing gear and flaps, has not yet been fully quantified.

Figure 9 shows the directivity patterns for the two independent cases and a comparison with Fink's prediction. Notice that landing gear noise radiates predominantly in the forward arc, peaking at 30 deg, a shallower angle than the one found for clean airframe.

The velocity index for landing gear noise could not be identified from the data available since all the related configurations corresponded to airspeeds closely clustered around 236 knots. Nevertheless, the literature shows a consensus for a value of 6 corresponding to the gear noise velocity index.[1,3]

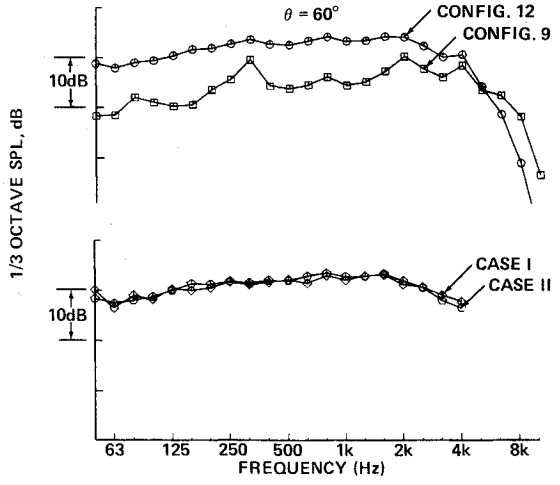

Fig. 8 Case II—isolation of landing gear component from subtraction of configuration 12 (0-deg flap, gear down, 238 knots, 2158 rpm) and configuration 9 (0-deg flap, gear up, 234 knots, 2172 rpm), and comparison with the component isolated in case I.

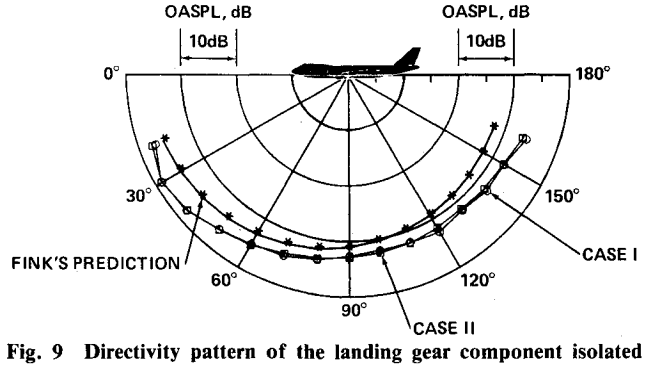

Fig. 9 Directivity pattern of the landing gear component isolated from two cases independently: Case I—logarithmic subtraction of configurations 11 and 8. Case II—logarithmic subtraction of configurations 12 and 9, and comparison with Fink's prediction at 236 knots.

Leading- and Trailing-Edge Flap Noise Components

Having isolated the clean airframe and landing gear components and established their velocity extrapolation indices, these can be used to isolate the leading- and trailing-edge flap noise components at three different settings: 30, 25, and 10 deg.

The 30-deg flap noise increment can be isolated for two different airspeeds, 196 and 145 knots from configurations 2 and 3, respectively. The isolation is achieved by extrapolating the clean airframe and gear noise components to the same airspeed and subtracting their addition logarithmically from the "dirty" configuration.

Figure 10 shows the isolated 30-deg flap component obtained by the procedure described above and its comparison to Fink's prediction for the case of 196 knots at $\theta = 60$ deg. Note that flap noise is radiated from a source of low frequency content. Fink's prediction matches the data very closely up to 500 Hz, thereafter it overpredicts by 2-3 dB.

Figure 11 depicts the directivity patterns of the 30-deg flap component isolated at two airspeeds independently. Note that both peak in the forward arc between 50 and 70 deg, with the difference in level due only to differences in airspeed. Their similarity is indicative of the same physical mechanism for noise radiation, adding confidence to the reliability of the measurements and the isolation procedure. Also shown is a comparison with Fink's prediction at 196 knots.

Since data were available at two airspeeds, it was possible to determine the velocity power index in the same manner that was done for the clean airframe component. The best collapse was found with a velocity index of 5 for the 30-deg flap component.

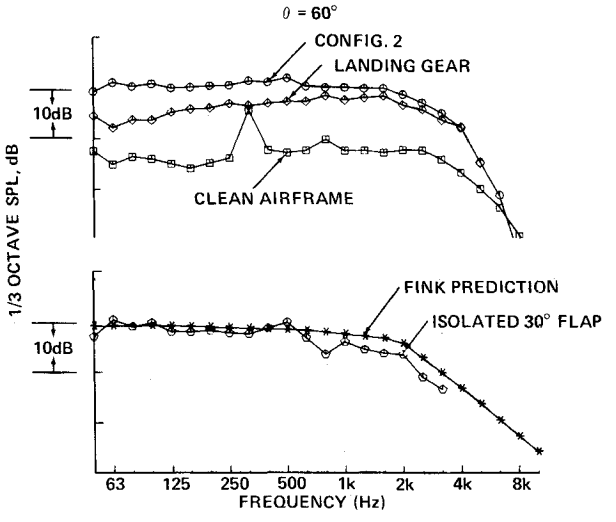

Fig. 10 Isolation of the 30-deg flap component (by subtraction of clean airframe and landing gear components, each extrapolated to 196 knots, from configuration 2) and comparison with Fink's prediction.

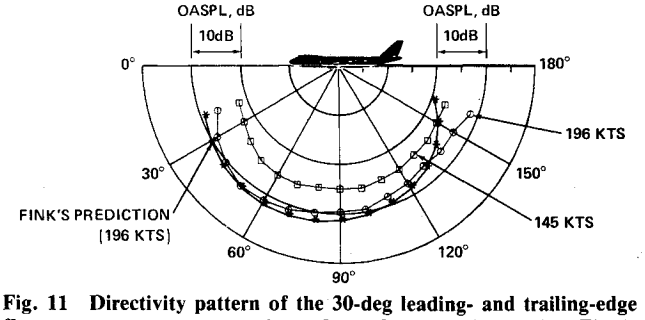

Fig. 11 Directivity pattern of the 30-deg leading- and trailing-edge flap component at two airspeeds and comparison with Fink's prediction at 196 knots.

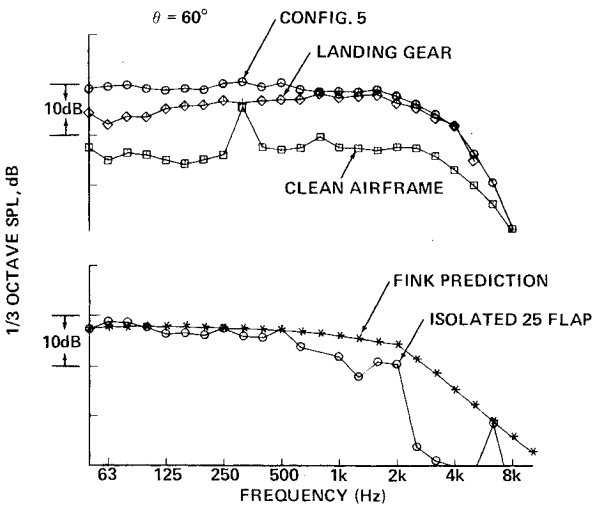

Fig. 12 Isolation of the 25-deg flap component (by subtraction of clean airframe and landing gear components, each extrapolated to 196 knots, from configuration 5) and comparison to Fink's prediction at $\theta = 60$ deg.

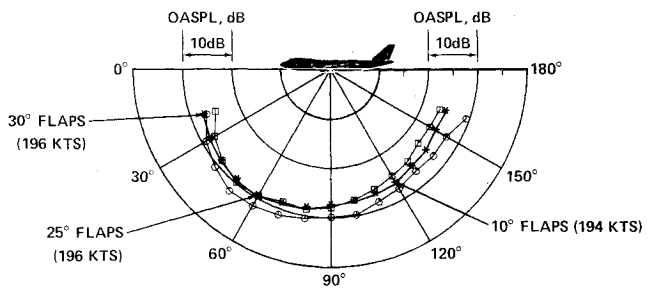

Fig. 13 Comparison of leading- and trailing-edge directivity patterns for three different flap settings: 30, 25, and 10 deg.

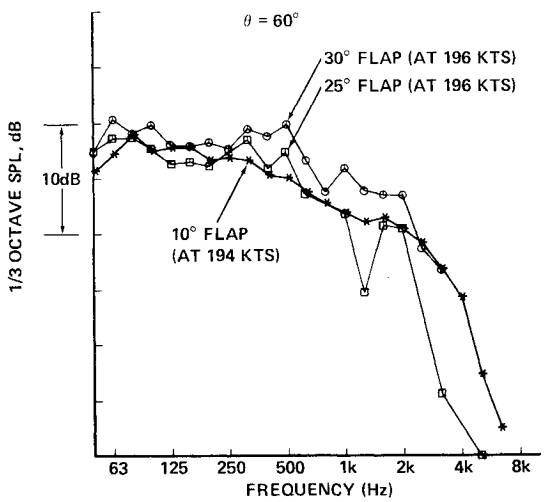

Fig. 14 Comparison of the leading- and trailing-edge flap components at three flap settings: 30, 25, and 10 deg.

The 25-deg flap noise component was isolated in a similar fashion from configuration 5 at 196 knots. Figure 12 shows the spectra from which it was isolated and its comparison to Fink's prediction. Figure 13 shows its directivity pattern compared to those isolated for the 30- and 10-deg flap components, at the same airspeeds. The difference in level (from the 30-deg flap component) results from the decrease in flap angle only, and the similarity in the radiation patterns suggests the presence of similar noise radiation mechanisms.

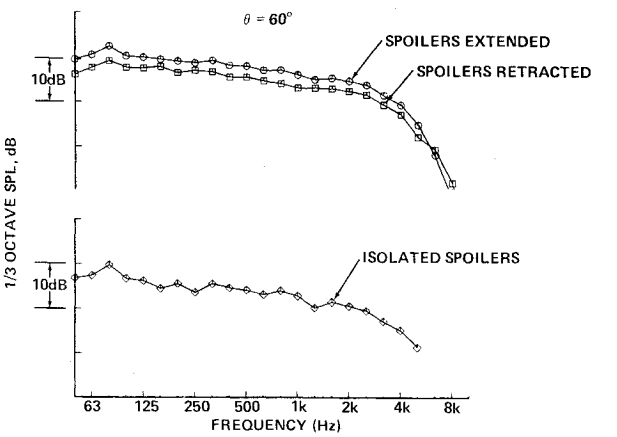

Fig. 15 Isolation of the spoilers noise component from subtraction of configuration 6 (spoilers extended, 10-deg flap, gear up, 200 knots, 1025 rpm) and configuration 7 (spoilers retracted, 10-deg flap, gear up, 194 knots, 1025 rpm), at $\theta = 60$ deg.

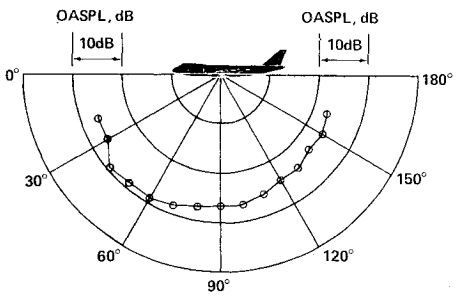

Fig. 16 Spoiler noise directivity pattern at 192 knots extrapolated to a constant radius of 394 ft with atmospheric absorption correction.

The latter statement also justifies the use of a velocity power index of 5 for the 25-deg flap component.

The 10-deg flap noise (Fig. 13) was isolated by subtracting the clean airframe component, extrapolated to 194 knots, from configuration 7 having the same airspeed.

Note that configuration 7 does not have the landing gear deployed, eliminating the possibility of gear-flap interaction noise contaminating the isolated 10-deg flap component. This is not the case for the 30- and 25-deg flap components which had the landing gear units deployed.

A comparison made between the 30-, 25-, and 10-deg flap components is depicted in Fig. 14, at $\theta = 60$ deg. The three components represent noise radiated from the leading- and trailing-edge flap system from aircraft approaching at very similar airspeeds; therefore differences in level should be attributed to the change in flap angle setting.

The 30- and 25-deg flap components depict distinct similarities in their spectral shapes. Following the trend that they set, one would expect the 10-deg flap component to be similar in shape and have a lower spectral level. Figure 14 shows this not to be the case, as the 10-deg flap component has a smoother behavior at low frequencies and higher levels than expected. Differences are also found in the directivity patterns, as was shown in Fig. 13. These differences are indicative of two different physical mechanisms. The 30- and 25-deg flap components were isolated from configurations having the landing gear deployed and show distinct tones at low frequencies. These tones can be associated with wake tones behind the gear strut. Alternatively, these can be attributed to the fan shaft rpm and its harmonics.

Spoilers

The noise radiated by the extension of the spoilers (obtained from configurations 6 and 7) caused an increase in level of

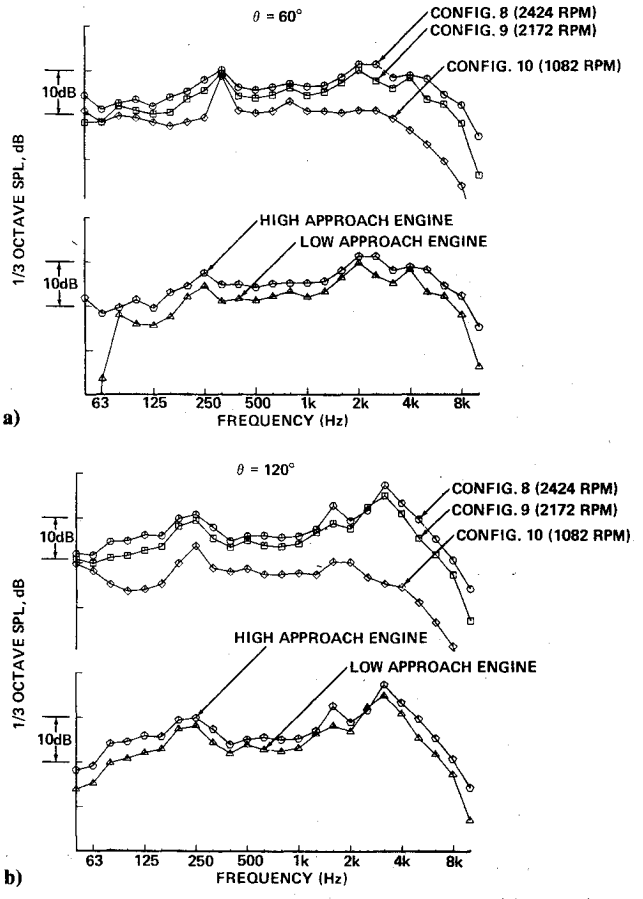

Fig. 17 a) Isolation of engine noise component at 234 knots in the forward arc. High approach engine from subtraction of configurations 8 (2424 rpm) and 10 (1082 rpm). Low approach engine from subtraction of configurations 9 (2172 rpm) and 10. b) Isolation of engine noise component at 234 knots in the aft arc. High approach engine from subtraction of configurations 8 (2424 rpm) and 10 (1082 rpm). Low approach engine from subtraction of configurations 9 (2172 rpm) and 10.

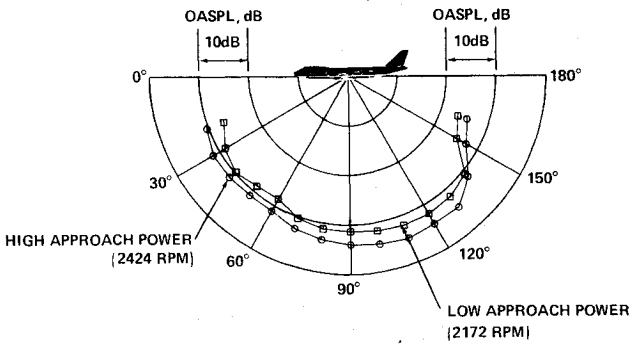

Fig. 18 Engine noise component—directivity pattern at 234 knots. Extrapolated to a constant radius of 394 ft with atmospheric absorption correction.

approximately 3 dB throughout the spectrum. That level increase is shown in Fig. 15 together with the isolated spectral shape. Note that it peaks at 80 Hz. Its directivity pattern (Fig. 16) is characterized by radiation into the forward arc, as was the case for other airframe noise sources.

Engine Noise

In order to assess the total noise radiated by the 747 aircraft at landing approach, it was necessary to isolate the engine noise component at the two specified approach powers.

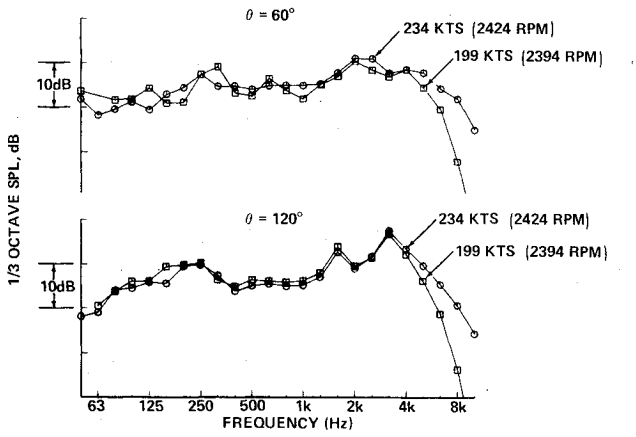

Fig. 19 Comparison of engine noise component at similar engine powers but different airspeeds, in the forward and aft arcs.

Table 2 Summary of the results with as-measured true airspeeds, velocity power indices and angles of peak OASPL, for each isolated component

Component	True airspeed, knots	Velocity index	Angle of peak OASPL, deg
Clean airframe (with tone)	233	4.5	40-60
Clean airframe (without tone)	278	4.5	30-50
Gear	236	6.0	30
Leading-edge and 30-deg trailing-edge flaps	196	5.0	50-60
Leading-edge and 30-deg trailing-edge flaps	145	5.0	60-70
Leading-edge and 25-deg trailing-edge flaps	196	5.0	50-60
Spoilers	192	...	40-50
High approach engine (2424 rpm)	234	...	110-120
Low approach engine (2172 rpm)	234	...	110-120

The engine component was isolated by subtracting configuration 10, depicting the clean airframe at the engine idle setting (1082 rpm), from configurations 8 and 9, containing the clean airframe with engines at the high (2424 rpm) and low (2172 rpm) approach powers, respectively. Figures 17a and 17b show the isolation of the engine component, in the forward and aft arc, from the above configurations, which were conducted at very close airspeeds, averaging 234 knots (see Table 1).

In reference to the clean airframe noise spectra, an important observation can be made by noting, from the top halves of Figs. 17a and 17b, the absence of any change in the tone frequency at 315 Hz when the engine rpm increases from 1082 to 2424, particularly in the forward arc. This is indicative of the nonpropulsive nature of the tone. In the aft arc, the engine noise sources become more dominant and the sound pressure levels increase throughout the spectra with increases in engine rpm. Figure 18 shows the directivity patterns for both power settings, with their peak levels radiating predominately in the aft arc, as expected.

Synthesis of Landing Approach Configurations

A summary table is presented in Table 2, with the as-measured true airspeeds, velocity power indices, and angles of peak OASPL. Configuration 1, in Table 1, represents a landing approach configuration not used for the isolation of

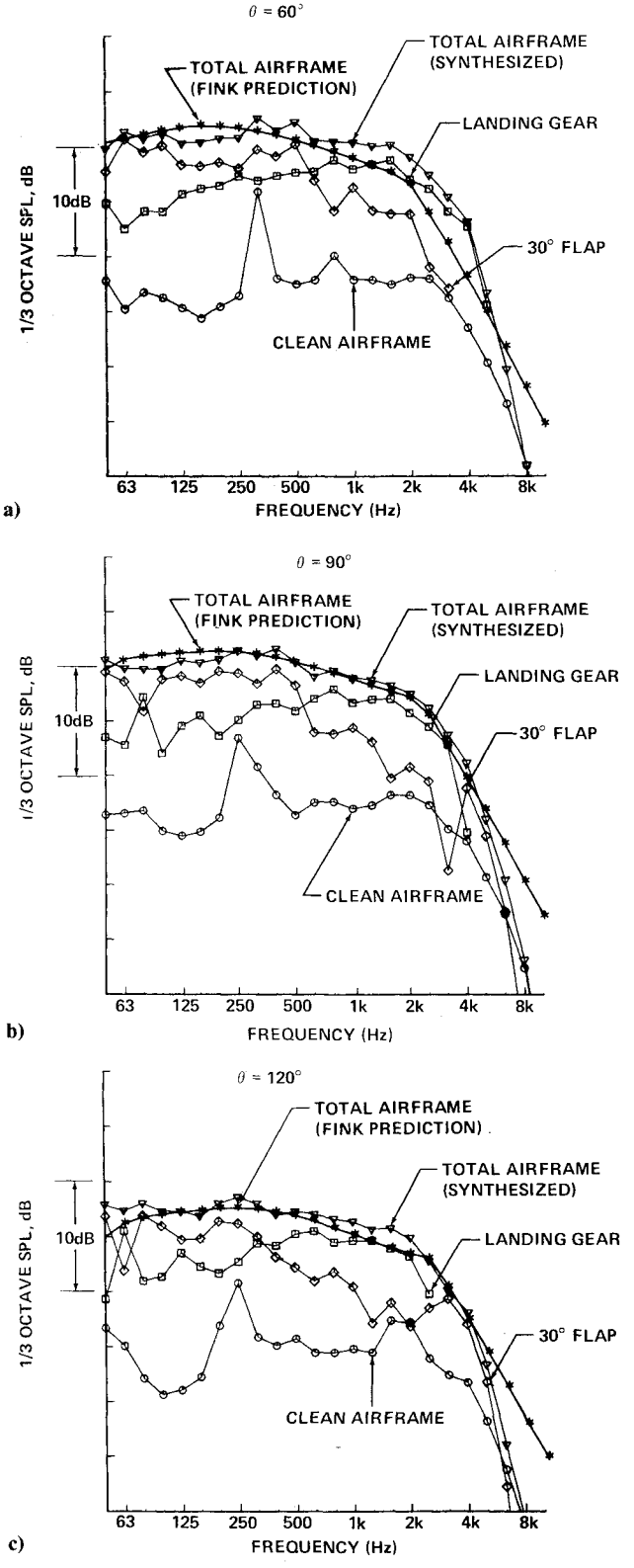

Fig. 20 Synthesis of the total airframe component for configuration 1, from isolated airframe noise components (clean airframe, landing gear, and 30-deg flap) and comparison with Fink's prediction at 199 knots.

any of the components. A main objective was to reconstruct this landing configuration from the independently isolated components.

Configuration 1 could be reconstructed from the logarithmic addition of the 30-deg flaps, gear and clean airframe noise components, each extrapolated with its own velocity index to 199 knots. The engine noise component for

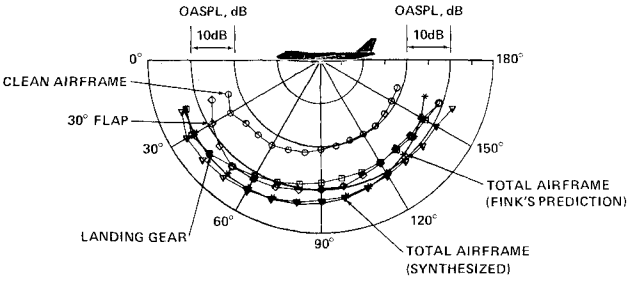

Fig. 21 Directivity pattern of the total airframe component for configuration 1, from isolated airframe noise components (clean airframe, landing gear, and 30-deg flap) and comparison with Fink's prediction at 199 knots.

the high approach setting was isolated from configurations 8 and 10, for a corresponding true airspeed of 234 knots. A comparison with the same component, isolated from configurations 1 and 2, at 199 knots is depicted in Fig. 19 and shows very small differences between the two in spectral shape and level despite the marked difference in airspeed. This justified the addition of the engine component at high approach power, with the higher airspeed, to the synthesis of configuration 1.

Figures 20a, 20b, and 20c show the individual airframe noise components, extrapolated with their corresponding velocity indices to 199 knots. Their logarithmic addition is the synthesized total airframe component and it is compared to Fink's prediction for $\theta = 60$, 90, and 120 deg, respectively. Figure 21 shows the directivity patterns of the airframe noise components with that of the synthesized total airframe compared to Fink's prediction. Figures 22a, 22b, and 22c show the synthesized total approach configuration as the sum of airframe and engine components, and it is compared to the actual flyover of configuration 1 for $\theta = 60$, 90, and 120 deg, respectively. The corresponding directivity patterns are shown in Fig. 23.

Notable agreement is found between the synthesized and actual spectra of configuration 1, at all directivity angles. This observation has important implications with respect to jet-flap interaction noise, as will be discussed in the following section. From the comparison between the total airframe and the engine components shown in Figs. 22a-c, it is clear that in the forward arc most of the noise radiated up to 2000 Hz is from airframe sources, while in the aft arc both components are more comparable in level.

Jet-Flap Interaction Noise for the 747-JT9D

All the individual airframe noise components were isolated from configurations which minimized the existence of jet-flap interaction (i.e., 0-deg flaps and/or idle engine power). It would be expected, then, that any jet-flap interaction noise present in the 747-JT9D at the approach power setting, will cause the spectral levels of the measured flyover to be higher than the synthesized levels. An increase is seen only at $\theta = 90$ deg, at low frequencies. Jet-flap interaction is likely to be dominant in the forward arc. Therefore the anomaly is probably due to the uncertainties inherent in flyover data which are highest at overhead and at low frequencies. Thus Figs. 22a-c suggest no evidence of jet-flap interaction noise.

EPNL Component Evaluation of the 747-JT9D at Approach

From the component isolation study described thus far, EPNL levels were computed for the individual airframe noise sources in order to assess, on a comparative basis, which source has the strongest impact on the community noise. For comparison, levels were also computed for the corresponding airframe noise components predicted from Fink's prediction method. In addition, the EPNL level was computed for the

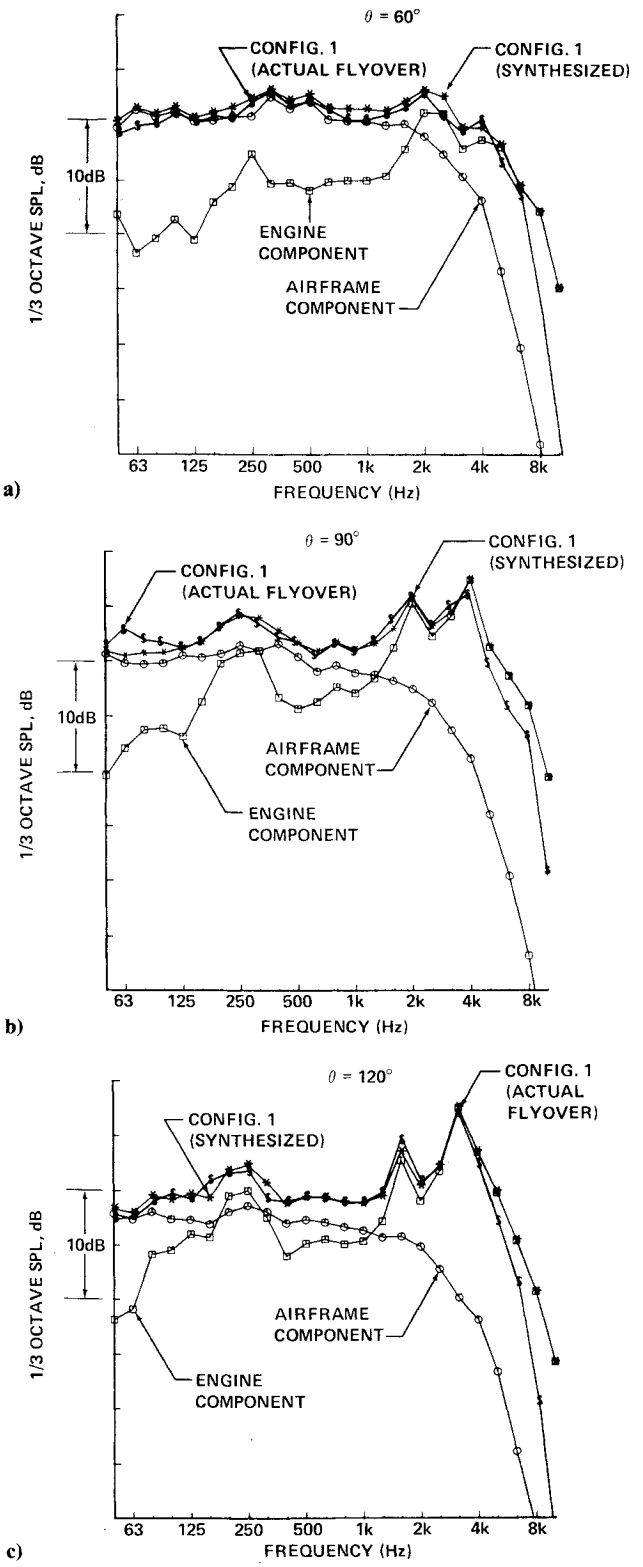

Fig. 22 Synthesis of approach configuration 1 from isolated airframe and engine components: 30-deg flap, gear down, high approach power (2408 rpm), and comparison to the actual flyover at 199 knots.

synthesized configuration 1, which simulates an approach condition, and it was compared to the level obtained for the actual flyover.

Figure 24 shows the EPNL breakdown of the components used to synthesize configuration 1 with the corresponding levels predicted by Fink's method (in unshaded columns) and the synthesized total approach level in comparison to the value obtained for the actual flyover.

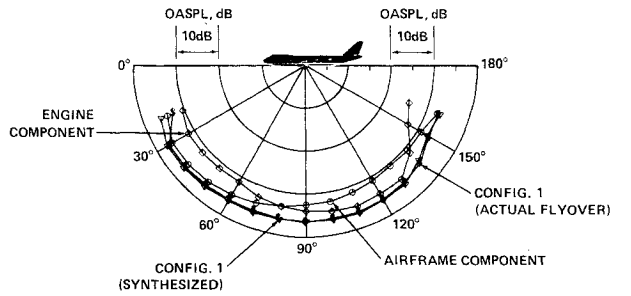

Fig. 23 Directivity pattern of the approach configuration 1, synthesized from isolated airframe and engine components: 30-deg flap, gear down, high approach power (2408 rpm), and comparison with the actual flyover at 199 knots.

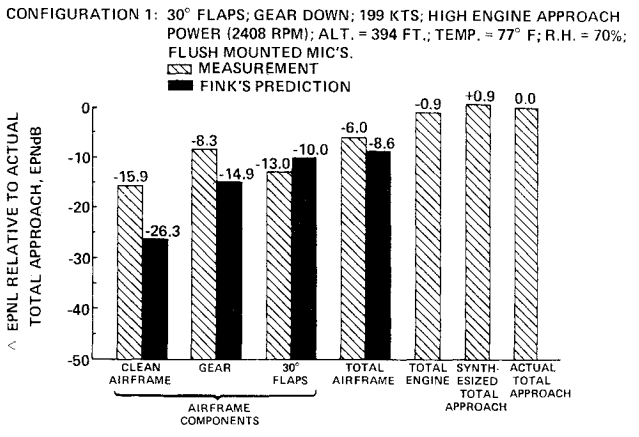

Fig. 24 EPNL component breakdown for the synthesis of configuration 1 with the corresponding levels predicted by Fink's method and a comparison between the synthesized total to the actual flyover approach level.

The results of this study show the landing gear as the major contributor to airframe noise as opposed to the 30-deg flap component predicted by Fink's method. Nevertheless, recall that the gear component was isolated from configurations with the leading- and trailing-edge flaps retracted. At approach, the leading- and trailing-edge flaps are deployed causing the flow around the wing gear strut and wheels to slow down and the wake generated to impinge on the trailing-edge flaps. This could alter the noise levels radiated from the landing gear as well as those from the flaps at approach. The extent of such interaction must be quantified. For this purpose, an additional flight configuration describing the contributions from the flap system with all the landing gear retracted is required, so that the landing gear noise component can be isolated from configurations having the flaps deployed. This is a subject of future investigation.

Conclusions

From the work presented herein, the following conclusions can be stated.

1 a) Spectral shapes and directivity patterns for the airframe noise components of the 747-JT9D aircraft have been accurately isolated from ensemble averaged flight test data; b) velocity power indices and angles of peak OASPL have been found consistent with theory; and c) from addition of individual components, the total noise radiated from the 747 during landing approach has been reconstructed, very accurately, in level, spectral shape and directivity pattern.

2) The data shows no significant evidence of jet-flap interaction noise for the 747-JT9D.

3) There is evidence of gear-flap interaction noise, possibly causing a reduction in noise levels and also the generation of tones at low frequencies.

4) The extension of the spoilers causes an increase in noise level of approximately 3 dB throughout the spectra. This noise source peaks in the low frequency range and its directivity pattern is characterized by radiation predominantly into the forward arc.

5) The results of this study show that the landing gear is the major contributor to airframe noise for the 747-JT9D aircraft. However, if the effect of flap deployment is included in the isolation of the landing gear noise component, the levels may be altered.

References

[1] Fethney, P. and Jelly, A.H., "Aircraft Self-Noise Studies on the Lockheed L-1011 Tristar Aircraft," AIAA 80-1061, June 1980.

[2] White, K.D., Lasagna, P.L., and Putnam, T.W., "Preliminary Measurements of Aircraft Airframe Noise with the NASA CV-990 Aircraft," NASA TMX-73, 116, Jan. 1976.

[3] Fink, M.R., "Airframe Noise Prediction Method," FAA-RD-77-29, March 1977.

[4] Paterson, R.W., Vogt, P.G., Fink, M.R., and Munch, C.L., "Vortex Noise of Isolated Airfoils," *Journal of Aircraft*, Vol. 10, May 1973, pp. 296-302.

[5] Tam, C.K.W., "Discrete Tones of Isolated Airfoils," *Journal of the Acoustical Society of America*, Vol. 55, June 1974, pp. 1173-1177.

[6] "Standard Values of Atmospheric Absorption as a Function of Temperature and Humidity," SAE, ARP-866A, March 1975.

[7] "Noise Standards: Aircraft Type Certification," Federal Aviation Regulations, Part 36, FAA, Dec. 1969.